



Optimized Design of an LCL Filter for Grid Connected Photovoltaic System and Analysis of the Impact of Neighbors' Consumption on the System

Chabakata Mahamat, Mickaël Petit, Francois Costa, Rym Marouani,
Abdelkader Mami

► To cite this version:

Chabakata Mahamat, Mickaël Petit, Francois Costa, Rym Marouani, Abdelkader Mami. Optimized Design of an LCL Filter for Grid Connected Photovoltaic System and Analysis of the Impact of Neighbors' Consumption on the System. Journal of Electrical Systems, 2017. hal-01676019

HAL Id: hal-01676019

<https://hal.archives-ouvertes.fr/hal-01676019>

Submitted on 5 Jan 2018

HAL is a multi-disciplinary open access archive for the deposit and dissemination of scientific research documents, whether they are published or not. The documents may come from teaching and research institutions in France or abroad, or from public or private research centers.

L'archive ouverte pluridisciplinaire **HAL**, est destinée au dépôt et à la diffusion de documents scientifiques de niveau recherche, publiés ou non, émanant des établissements d'enseignement et de recherche français ou étrangers, des laboratoires publics ou privés.

**Optimized Design of an LCL Filter for Grid
Connected Photovoltaic System and
Analysis of the Impact of Neighbors'
Consumption on the System**

This paper presents an optimized design method for an LCL filter for a grid connected photovoltaic system. This method is based on the Fast Fourier Transform (FFT) of the current and voltage which provides the current ripples thus allowing to find the LCL filter passives elements. A trick which consists of inductances fragmentation is adopted in order to reduce the volume and the cost of the filter. Then, we do an analysis taking into account the impact of our neighbors consumption. This system is controlled by a decoupled active and reactive power control (PQ control) using a Phase Locked Loop (PLL) for the system's synchronization. Finally, we present and discuss the results of our simulation obtained by Matlab software (simulink and simpowersystems) in order to highlight the proposed study.

Keywords: Optimized design; LCL filter; grid connected photovoltaic system.

Article history: Received 13 July 2017, Accepted 19 October 2017

1. Introduction

In a grid connected photovoltaic (*PV*) system, an inverter between the *PV* source and the utility grid is required. It is necessary to insert a passive filter between the inverter and the utility grid in order to filter the harmonics produced by the inverter [1], [2].

There are three types of passive filter : the *L* filter, the *LC* filter and the *LCL* filter. Nowadays, the *LCL* filter is vastly used than the others because of its filtering efficiency as in [1], [2], [3], [4], [5], [6], [7], [8] and [11].

However, many authors impose simplifying hypotheses in which they connect the neutral of the utility grid to the midpoint of the *DC* bus and consider the inverter as a *DC/DC* converter to find the current ripple expression as a function of inductance, switching frequency, *DC* bus voltage and duty cycle. Knowing the ripple formula allows to find the inductance on the inverter side L_1 . The value of the capacitor C is found using the formula of the reactive power generated by the capacitor. Very often, a variation of the reactive power lower than 5% of the active power is considered, as in [1], [2], [3] and [4]. Then, knowing L_1 and C , and by using the transfer function of the *LCL* filter, it is easy to find the grid side inductance L_2 .

This is practically the most common method for calculating *LCL* filter elements, but it is based on unrealistic assumptions. Indeed, in the case of the inverter, the duty cycle changes

* Corresponding autor: Chabakata Mahamat, chabakata.mahamat@satie.ens-cachan.fr

¹ Université de Paris-Saclay, Ecole Normale Supérieure (ENS) de Paris-Saclay, Laboratoire SATIE, France

² Université de Tunis El Manar, Faculté des Sciences de Tunis, Laboratoire LAPER, Tunisie

³ Conservatoire national des arts et métiers (Cnam) Paris, CNRS, Laboratoire SATIE, France

⁴ Université de Paris Est Créteil, ESPE de Créteil, Laboratoire SATIE, France.

emails: chabakata.mahamat@satie.ens-cachan.fr, mickael.petit@satie.ens-cachan.fr

francois.costa@satie.ens-cachan.fr, rimarouani@yahoo.fr, abdelkader.mami@fst.utm.tn.

over time, the output voltage of the inverter is also a function of time and depends on the grid voltage. In addition, connecting the utility grid neutral to the midpoint of the DC bus makes easier the calculation by setting the common mode voltage to null; Despite its easiness, from an economical point of view, this solution is not desirable because it requires an additional cable. On the other hand, if the neutral is not connected to the midpoint, the expression of the current ripples becomes very complicated because it is necessary to take account of the common mode voltage [5].

The objectives of this paper are to design the LCL filter according to the requirements of the *IEEE1547* [13], taking into account the common mode voltage, and using a design method based on the Fast Fourier Transform (FFT) of the currents and voltages on the one hand, and to analyze the system by taking into account the impact of the consumption of neighbors on our system on the other hand. In order to optimize the magnetic design of the filter inductances, we apply a trick consisting of dividing each inductance value and making it in several small inductances in series. This technique makes it possible to choose small inductances cores at low cost and less bulky. It is shown that there is a gain on the overall volume and on the manufacturing cost of these inductances.

A decoupled active and reactive power control (PQ control) will be used to control the current to be injected into the utility grid and to adjust the output voltage of the inverter. The synchronization of the system is done by a Phase-Locked Loop (PLL).

This paper is organized around the following sections: Section 2 describes the system, section 3 presents the modeling of the system, section 4 and 5 present the design of the LCL filter. Finally, section 6 presents the simulation results and discussion.

2. Description of the system

The diagram of the grid connected PV system is shown in figure 1. It is composed of the photovoltaic generator (PVG), the three-phase inverter, the LCL filter and the utility grid. A damping resistance R_f is added in series with the filter capacitor in order to limit the resonance effects of the filter [6], [7], [8]. This resistance can also be connected in parallel with the capacitor. Moreover, there are other types of damping such as active damping or other types of passive damping, but we have chosen here the simplest case, namely the passive damping obtained by adding of the resistance in series with the capacitor. The RL load represents the consumption of our neighbors which are connected on the same grid as our system.

The PVG provides a continuous energy that will be converted into alternative form by the inverter before injecting it into the grid through the LCL filter. The PVG will not be studied here, it will therefore be replaced by a DC voltage source (V_{dc}) which is the input voltage of the inverter. The system is controlled by a decoupled PQ control which is based on the Park transform, the current control in the Park frame, the decoupling of the direct and quadrature (I_{dq}) components of the current and the grid voltage compensation. A Phase-Locked Loop (PLL) is used to synchronize the system with the utility grid. First, we are interested in the modeling and design of the LCL filter before returning to the analysis and control of the system.

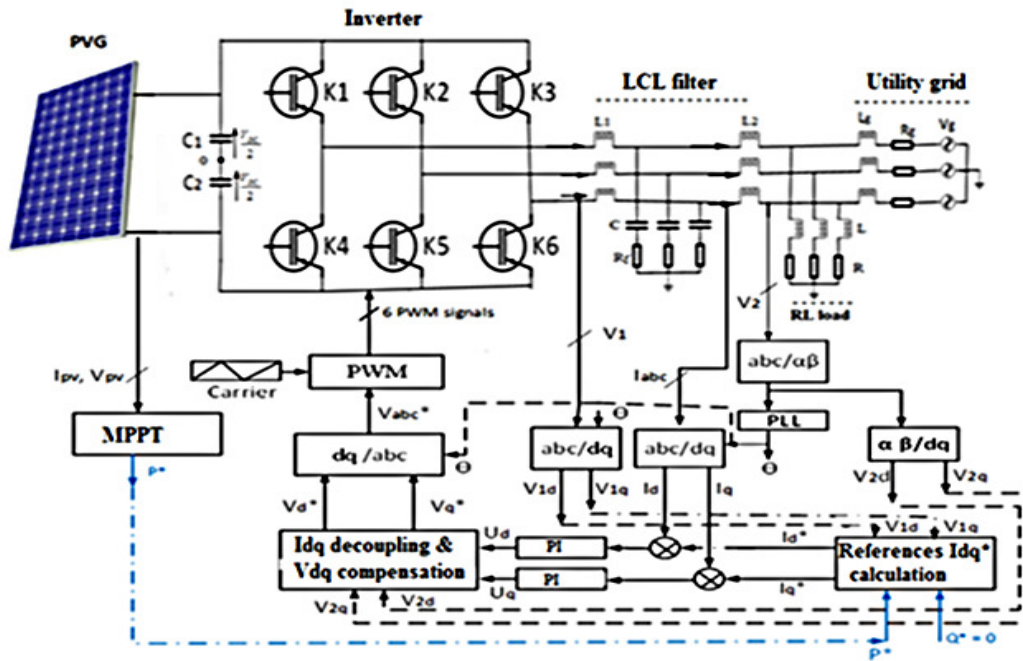


Figure 1. Diagram of the grid-connected PV system and its control loop

3. Modeling of the LCL filter

By replacing the *PVG* by the *DC* voltage (V_{dc}), by ignoring the control scheme and the load *RL*, the diagram of figure 1 becomes that of figure 2. To simplify, we create a fictitious neutral "0" (midpoint) by dividing V_{dc} .

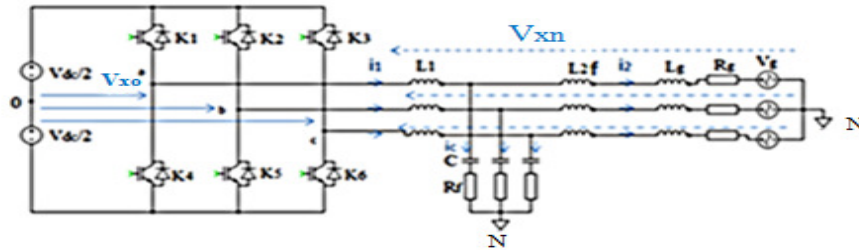


Figure 2. Simplified diagram of the system

The mathematical equations governing the behavior of this scheme are the following:

$$\begin{cases} V_{x0} = \frac{V_{dc}}{2}, \text{ if } K_i = 1 \text{ and } K_i' = 0 \\ V_{x0} = -\frac{V_{dc}}{2}, \text{ if } K_i = 0 \text{ and } K_i' = 1 \end{cases} \quad (1)$$

With $x = a, b, c$ and $i = 1, 2, 3$

4. Electrical design of the LCL filter

To simplify, we set : $V_{xn} = V_1$, $L_2 = L_{2f} + L_g$ et $V_g = V_2$. The simplified diagram of the *LCL* filter can be represented in single-phase as shown in figure 3. The internal resistances (R_1 and R_2) are neglected in this diagram. Where, V_1 is the line-to-phase inverter voltage and V_2 is the line-to-phase grid voltage.

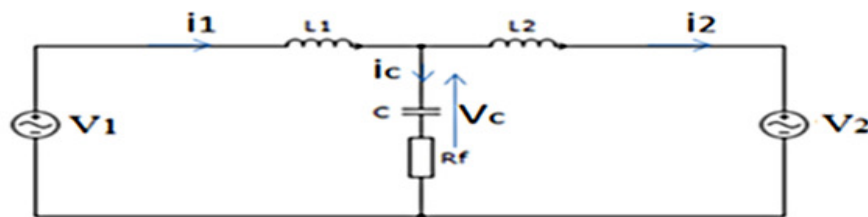


Figure 3. Topologie of the LCL filter

The transfer function of the *LCL* filter is given in (2) [6], which expresses the resonance pulsation (ω_{res}) and damping resistor R_f in (3).

$$H(s) = \frac{I_2(s)}{V_1(s)} = \frac{C_f R_f s + 1}{L_1 C L_2 s^3 + C(L_1 + L_2) R_f s^2 + (L_1 + L_2)s} \quad (2)$$

$$\begin{cases} \omega_{res} = \sqrt{\frac{L_1 + L_2}{L_1 C L_2}} \\ R_f = \frac{2z\omega_{res}L_1L_2}{L_1 + L_2} = \frac{2z}{\omega_{res}C} \end{cases} \quad (3)$$

Where ω_{res} is the resonance pulsation ($f_{res} = \frac{\omega_{res}}{2\pi}$), z is the damping factor and s is the Laplace variable.

In the literature, it is often mentioned that the resonant frequency must respect (4) in order for there to be stability of the system.

$$10 f < f_{res} < 0.5 f_{sw} \quad (4)$$

4.1. Constraint of the reactive power variation and calculation of C

The value of the capacitor C is chosen so as to maximize the power factor [3]. For this purpose, the reactive power generated by this capacitor must be less than or equal to five percent of the rated active power of the installation ($Q_c \leq 5\% \cdot P_n$). The reactive power formula is given in (5).

$$Q_c = C \cdot \omega \cdot U_n^2 \quad (5)$$

Either the expression of a single capacitor:

$$C_{max} = \frac{0.05 \cdot P_n}{3 \cdot 2\pi f \cdot U_n^2} \quad (6)$$

Where P_n rated power, f grid frequency and U_n phase-to-phase grid rated voltage.

4.2. Voltage drop constraint and determination of total inductance L

By neglecting the capacitor C , the voltage drop module is shown in (7).

$$\Delta V_L = L \cdot \omega \cdot I \quad (7)$$

where L is the total inductance ($L = L_1 + L_2$), ΔV_L is the voltage drop at this inductance, I the rated current and ω is the grid pulsation ($\omega = 2\pi f$).

We admit $\Delta V_L = 10\% \cdot V$ of voltage drop to satisfy the *IEEE1547* standard [13].

$$I = \frac{P_n}{3 \cdot V} \quad (8)$$

$$L = \frac{10\% \cdot 3 \cdot V}{\omega \cdot P_n} \quad (9)$$

Where V is the line-to-phase grid rated voltage ($V = 220$ V).

4.3. Constraints of current ripples

The maximum current ripple on the inverter side is generally chosen to be between 10% and 20% of the rated current, whereas the maximum grid ripple must be less than or equal to 0.3% [13].

$$10\% \cdot I \leq \Delta I_{1m} \leq 20\% \cdot I \quad (10)$$

$$\Delta I_{2m} \leq 0.3\% \cdot I \quad (11)$$

In the simplified model, the three-phase grid voltage is denoted V_2 . In reality, it is a three-phase voltage vector forming a balanced three-phase system that is regularly shifted by $\frac{2\pi}{3}$. If only one phase is considered (e.g. phase a), the formula of V_2 is that of (12).

$$V_2 = V\sqrt{2} \sin(\omega t) \quad (12)$$

By considering (1), the curve of $V_{a0}(t)$ is plotted in figure 4.

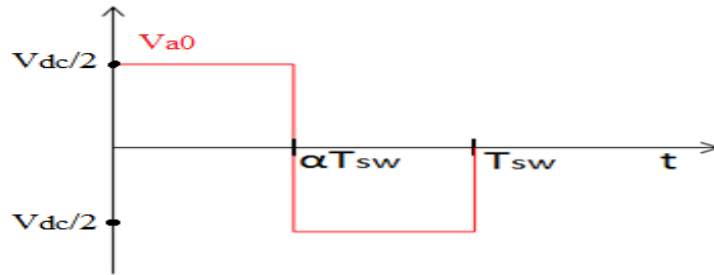


Figure 4. Evolution of the inverter voltage over time

The mean value of the inverter voltage is calculated in (13).

$$V_{a0_moy} = \frac{1}{T_{sw}} \int_0^{T_{sw}} V_{a0}(t) dt = \frac{V_{dc}}{2} [2 \cdot \alpha(t) - 1] \quad (13)$$

The formula of the duty cycle is given in (14)

$$\alpha(t) = \frac{1}{2} + \frac{m}{2} \sin(\omega t + \varphi) \quad (14)$$

By injecting (14) into (13) we obtain (15).

$$V_{a0_moy} = \frac{m \cdot V_{dc}}{2} \sin(\omega t + \varphi) \quad (15)$$

where φ is the phase shift between the grid voltage and the inverter voltage, T_{sw} is the switching period.

From (15), (16) is deduced.

$$V_{a0_eff} = V_1 = \frac{V_m}{\sqrt{2}} = \frac{m V_{dc}}{2\sqrt{2}} \quad (16)$$

On the other hand, since the capacitor is very low (1.5 μ F), the current passing through it (I_c) is negligible compared to current passing into the grid (I_2). So by neglecting I_c in figure 3, the system can be represented in a Fresnel diagram as in figure 5 ($I_1 = I_2 = I$).

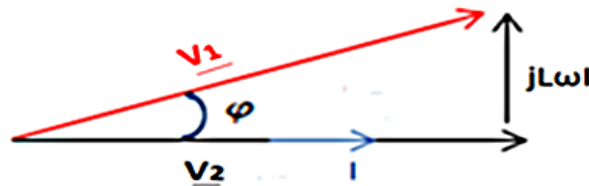


Figure 5. Fresnel diagram of the system connected to the network (phase a)

From figure 5, equation (17) can be written.

$$\underline{V}_1 = \underline{V}_2 + jL\omega I \quad (17)$$

$$|V_1| = V_1 = \sqrt{V_2^2 + (L\omega I)^2} \quad (18)$$

Where $V_2 = V$ is the rated grid voltage and j is the complex operator.

By using (16) and (18), we obtain (19).

$$m = \frac{2\sqrt{2} \cdot \sqrt{V^2 + (L\omega I)^2}}{V_{dc}} \quad (19)$$

m is the depth of modulation.

By placing the expression of m of equation (19) in equation (15) we find (20).

$$\alpha(t) = \frac{1}{2} + \frac{2\sqrt{2} \cdot \sqrt{V^2 + (L\omega I)^2}}{2V_{dc}} \cdot \sin(\omega t + \varphi) \quad (20)$$

$$\varphi = \arctan\left(\frac{L\omega I}{V}\right) \quad (21)$$

We have already mentioned that we will opt for the calculation of current ripples by using the *FFT*. For this, figure 3 becomes figure 6 which takes account of admittances.

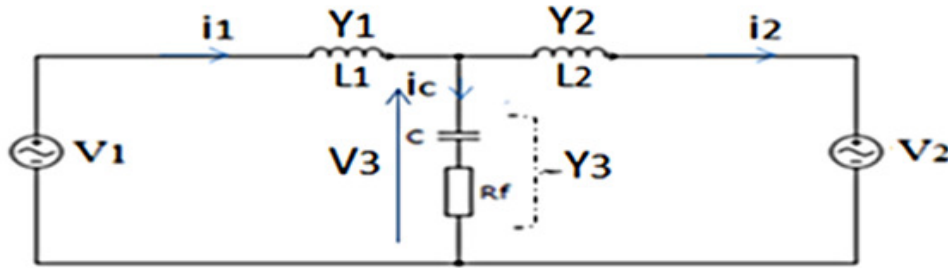


Figure 6. Modified diagram of the LCL (admittances)

By applying the Millman theorem, the formula of the common voltage (V_3) is given in (22).

$$V_3 = \frac{V_1 Y_1 + V_2 Y_2}{Y_1 + Y_2 + Y_3} \quad (22)$$

$$\begin{cases} Y_1(\omega_h) = \frac{1}{jL_1\omega_h} \\ Y_2(\omega_h) = \frac{1}{jL_2\omega_h} \\ Y_3(\omega_h) = \frac{1}{R_f + \frac{1}{jC\omega_h}} \end{cases} \quad (23)$$

Where ω_h is the harmonic pulsation. The formula of currents (i_1 and i_2) taking into account all frequencies (fundamental and harmonics) are given in (24).

$$\begin{cases} i_1(\omega_h) = \frac{V_1 - V_3}{jL_1\omega_h} \\ i_2(\omega_h) = \frac{V_3 - V_2}{jL_2\omega_h} \end{cases} \quad (24)$$

The *FFT* of the current is done in (25).

$$\begin{cases} FFT(i_1) = \frac{FFT(V_1) - FFT(V_3)}{jL_1\omega_h} \\ FFT(i_2) = \frac{FFT(V_3) - FFT(V_2)}{jL_2\omega_h} \end{cases} \quad (25)$$

The system parameters are given in Table 1.

Table 1: Parameters of the grid connected PV system

Symbol	Parameter	Value	Unit
P_n	Rated power	5.2	kVA
I	Rated current	7.87	A
V	Rated line-to-phase grid voltage	220	V
U_n	Rated phase-to-phase grid voltage	381	V
V_{dc}	DC voltage	750	V
f_{sw}	Switching frequency	20	kHz
f	Grid frequency	50	Hz
ω	Grid pulsation	$2\pi f = 100\pi$	rad/s
ΔI_{1m}	Maximum inverter current ripples	$20\% \cdot 7.87 = 1.57$	A
ΔI_{2m}	Maximum grid current ripples	$0.3\% \cdot 7.87 = 23.6$	mA
ΔV_{Lm}	Voltage drop	$\Delta V_{Lm} = 10\% \cdot 220 = 22$	V
C_m	Maximum capacitor	2	μF
L_T	Total inductance	8.8	mH
L_1	Inverter side inductance	to be find	mH
L_2	Grid side inductance	to be find	mH
C	Optimal capacitor of the filter	to be find	μF
R_f	Damping resistance	to be find	Ω

In order to find the unknown elements of table 1, we must answer the following question. What are the optimal values of L_1 , L_2 and C to respect the following constraints ? $L = L_1 + L_2 \leq 8.8$ mH, $C \leq 2$ μF , $\Delta I_{1m} \leq 1.57$ A et $\Delta I_{2m} \leq 23.6$ mA.

For this, we have written a Matlab program with which we plot the three-dimensional curves of the maximum grid current ripple (ΔI_{2m}) as a function of L_1 , L_2 and C (R_f is neglected here), by varying L_1 and L_2 from 1mH to 8.8 mH for different values of C between 1 μF and 2 μF . Only the standardized values of unpolarized capacitors (E12) are considered here. The Matlab program indicates that the best case is where $C = 1.5$ μF and two symmetrical values of L_1 and L_2 (3 mH, 3.5 mH) or (3.5 mH, 3 mH) as shown in figure 7 (X corresponds to L_1 , Y corresponds to L_2 and Z corresponds to ΔI_{2m}).

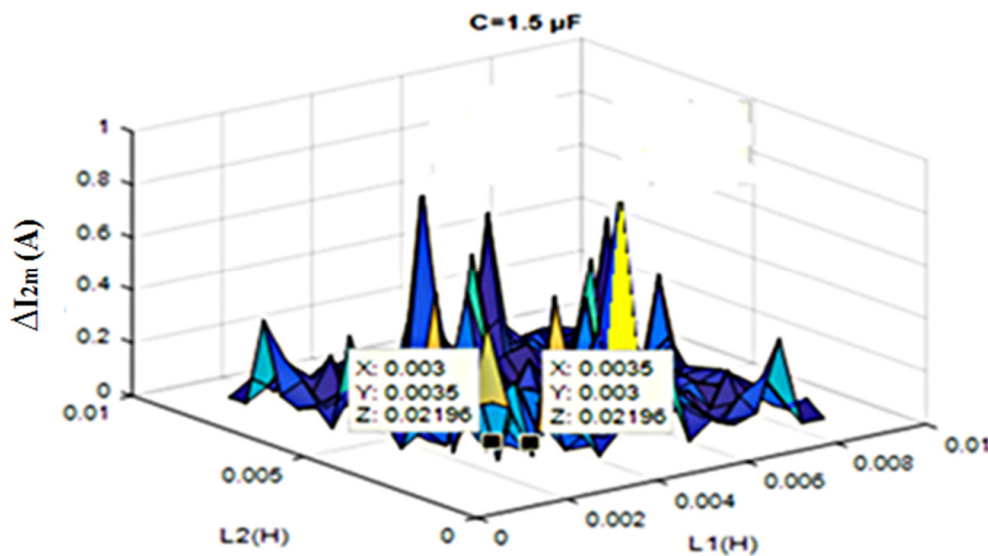


Figure 7. Grid current ripples ΔI_{2m} vs L_1 , L_2 and C

At this level, it is not possible to know which of L_1 or L_2 should be preferred. To find out, the curve of the maximum inverter current ripples (ΔI_{1m}) is plotted in figure 8 (here, X corresponds to L_1 , Y corresponds to L_2 and corresponds to ΔI_{1m}).

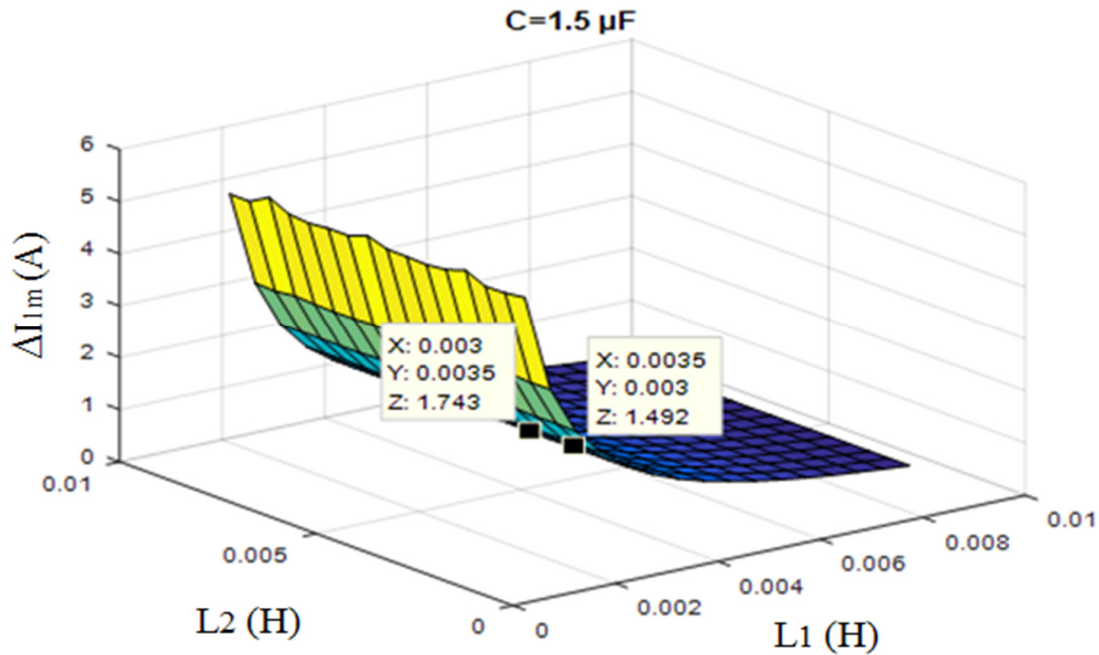


Figure .8 Inverter current ripples ΔI_{1m} vs L_1 , L_2 and C

According to figure 8, the maximum inverter current ripple is lower ($\Delta I_{1m} = 1.492$ A) when $L_1 = 3.5$ mH and $L_2 = 3$ mH than when $L_1 = 3$ mH and $L_2 = 3.5$ mH ($\Delta I_{1m} = 1.743$ A). On the other hand, the maximum grid current ripple is the same in both cases ($\Delta I_{2m} = 22$ mA). Therefore, the optimal values of the LCL filter parameters are : $L_1 = 3.5$ mH, $L_2 = 3$ mH and $C = 1.5$ μ F.

With these values, we find $\omega_{res} = 20315$ rad/s and $f_{res} = 3233$ Hz. $500\text{Hz} < 3233 \text{ Hz} < 10000 \text{ Hz}$. The stability condition of equation (6) is satisfied.

To determine R_f , we vary z between $[0, 1]$ using (3) and we find table 2.

Table 2: Damping resistance value

Damping factor z	Damping resistance R_f (Ω)
0	0
0.0588	3.86
0.166	10.89
0.707	46.4
1	65.63

Then, we tested these different values (see table 2) and we found that the optimal value of the damping resistance is $R_f = 3.86 \Omega$. Because this value does not modify the current ripples. Figures 9 and 10 show the ripples of the grid current and inverter current

respectively, when R_f is taken into account. We find practically the same values when we neglected R_f .

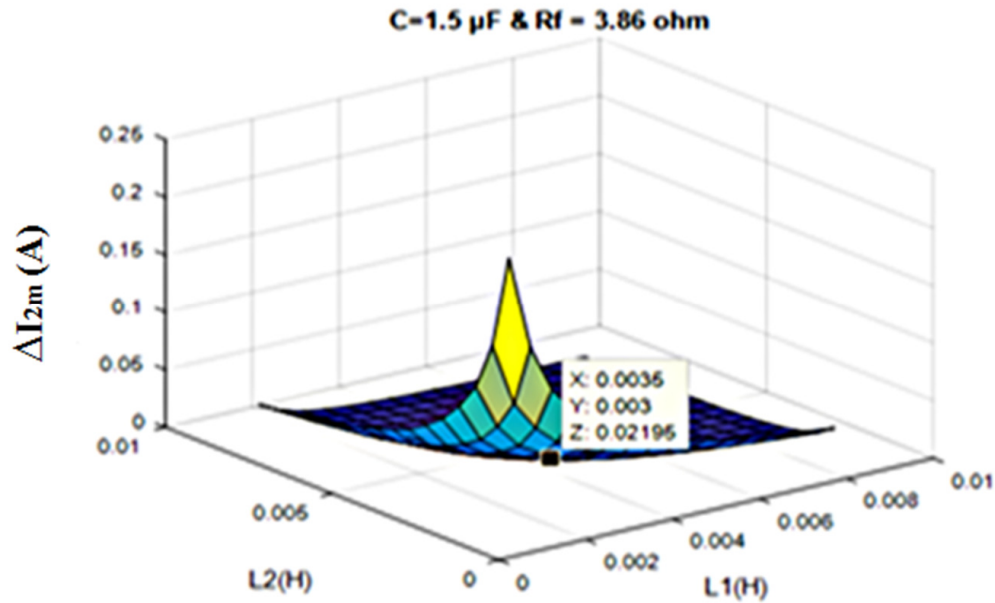


Figure 9. Grid current ripples ΔI_{2m} vs L_1 , L_2 , C and R_f

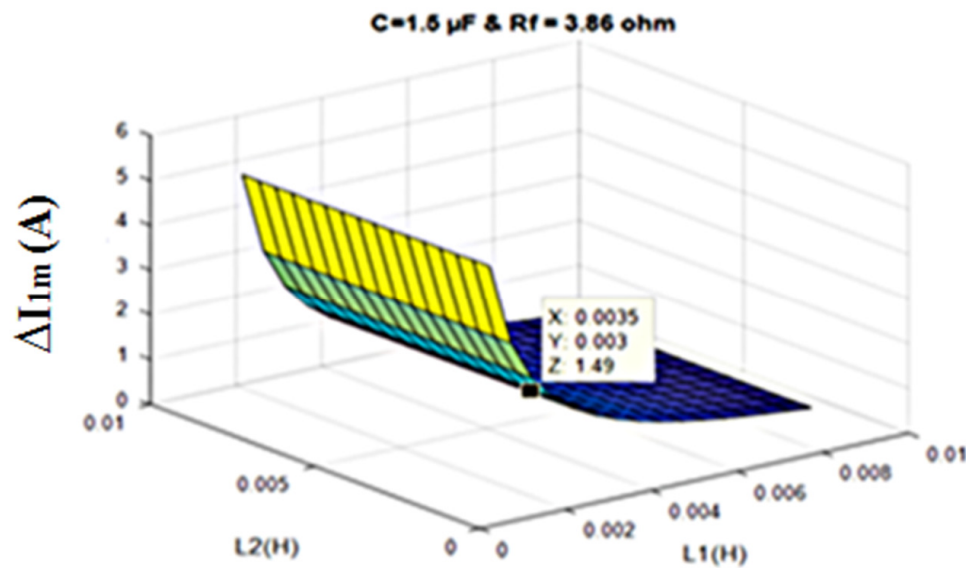


Figure 10. Inverter current ripples ΔI_{1m} vs L_1 , L_2 , C and R_f

The Bode diagram of the *LCL* filter is then shown in figure 11. Figure 11 shows that the insertion of the resistance R_f in series with the capacitor made it possible to suppress the peak due to the resonance phenomenon (curve in red).

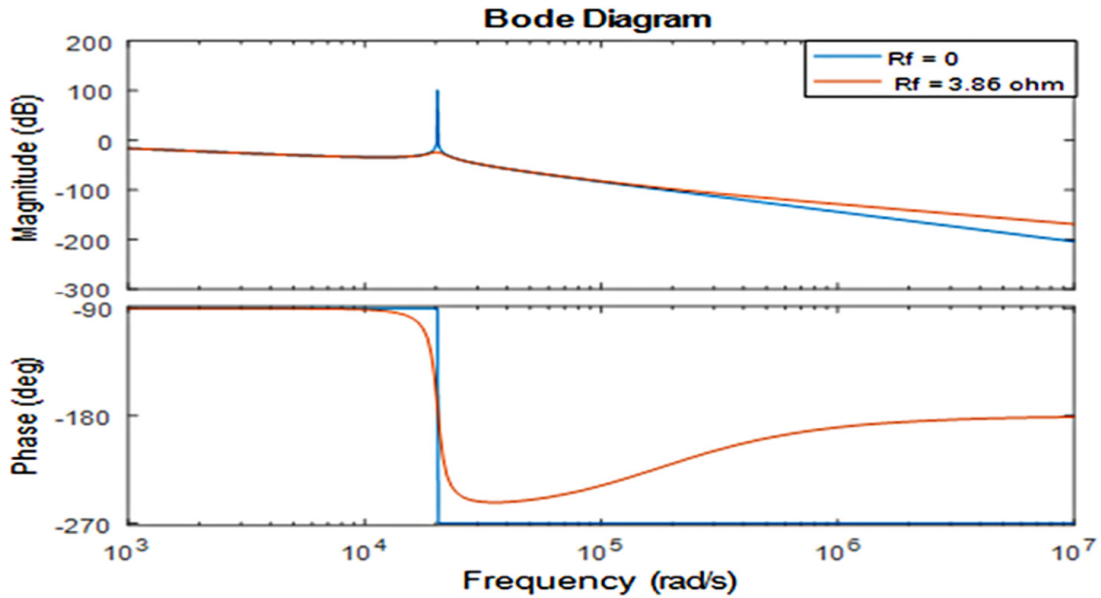


Figure 11. Bode diagram of the undamped LCL filter ($R_f = 0 \Omega$) and damped LCL filter ($R_f = 3.86 \Omega$)

5. Magnetic design of the filter inductances

Knowing the values of the passive components L_1 and L_2 , we are interested in the magnetic design which consists in determining the magnetic core, the number of turns, the air gap, joules losses, iron losses and the temperature evaluation of each inductance. Our magnetic design method is based on the areas product method presented in [15]. The design method is summarized in the flowchart (see figure 12) gives the results of table 3. These results are obtained using a Matlab program.

Table 3: Inductance parameters design

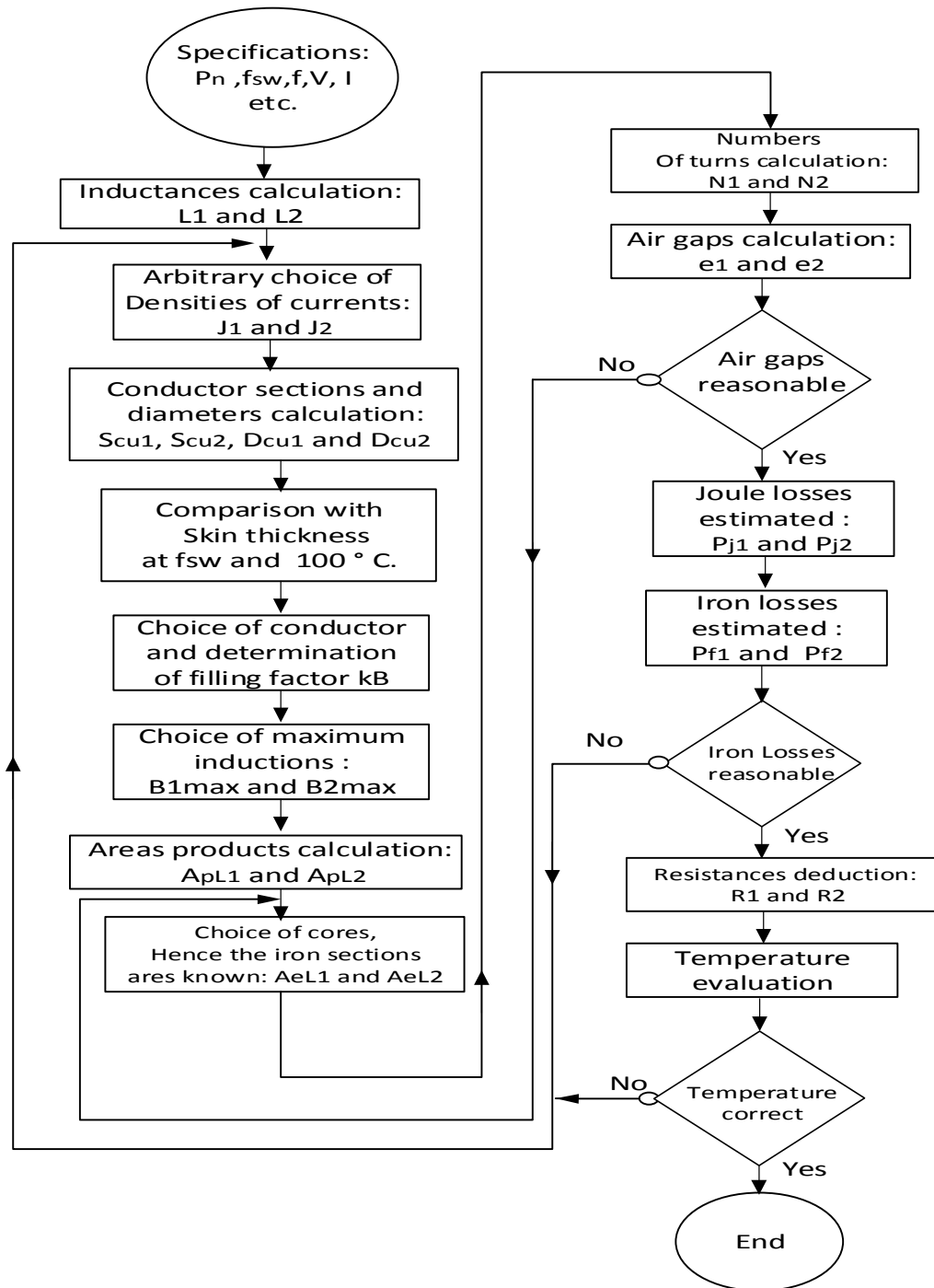
Symbol	Parameter	Value	Unit
N_1	Number of turns of inductance L_1	81	
N_2	Number of turns of inductance L_2	71	
e_1	Air gap of inductance L_1	4.3	mm
e_2	Air gap of inductance L_2	3.3	mm
P_{j1}	Joule losses in inductance L_1	14.24	W
P_{j2}	Joule losses in inductance L_2	10.98	W
P_{f1}	Iron losses in inductance L_1	11	kW
P_{f2}	Iron losses in inductance L_2	10.9	kW
R_1	Winding resistance of L_1	0.46	Ω
R_2	Winding resistance of L_2	0.36	Ω
ΔT_1	Temperature difference in L_1	57	$^{\circ}\text{C}$
ΔT_2	Temperature difference in L_2	52	$^{\circ}\text{C}$

In hot countries like Chad, $T_{max} = 100^{\circ}\text{C}$ and $T_{amb} = 40^{\circ}\text{C}$ can be considered. This gives $\Delta T = 60^{\circ}\text{C}$.

According to table 3, L_1 is designed to operate at ambient temperature $T_{amb1} = 43^{\circ}\text{C}$ ($T_{amb1} = T_{max} - \Delta T_1$) and L_2 at the ambient temperature $T_{amb2} = T_{max} - \Delta T_2 = 48^{\circ}\text{C}$. So these inductances are well designed to operate in Chad.

When we choose the cores for inductances L_1 and L_2 , we found that only the ferrite core PM114 [16] is suitable. Because it has a areas product ($A_p = 1840400 \text{ mm}^4$) greater than

those calculated (for L_1 , $A_{pL1} = 829800 \text{ mm}^4$ and for L_2 , $A_{pL2} = 640000 \text{ mm}^4$). However, this core costs too much (176.90 euros, at Distrelec) and are too bulky ($V_{pm114} = 334000 \text{ mm}^3$). In order to reduce the manufacturing cost and the volume of the passive components (L_1 and L_2), we said why not split each inductance and realize it in several small inductances in series? In this case, the optimum in terms of volumes is found when each inductance is divided by two and two *PM87* cores are chosen for L_1 and two *PM74* cores for L_2 as shown in figure 13. On the other hand, the *PM87* core costs 63 euros and the *PM74* costs 68 euros. So by dividing the inductances and choosing two small cores, there is a gain of 50.9 euros for L_1 and 34.9 euros for L_2 for one inductance. For three phase *LCL* filter, the cost is multiplied by three.

Figure 12. Flowchart of the design procedure of L_1 and L_2

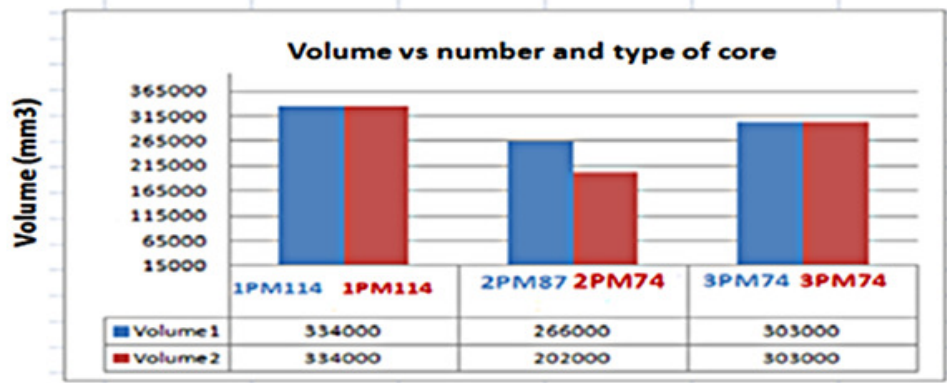


Figure 13. Impact of core choice on inductances volume

We can see in figure 13 that, at the optimum, the volume of the inductance L_1 is equal to : $Volume_1 = 2 \cdot V_{PM87} = 266000 \text{ mm}^3$ and the volume of L_2 is equal to : $Volume_2 = 2 \cdot V_{PM74} = 202000 \text{ mm}^3$ [16].

6. Simulations results and discussion

6.1. Simulations results

Now that the *LCL* filter elements are known, we can look at the control of the system and its analysis taking into account the impact of the consumption of our neighbors. The system control diagram is shown in figure 1. It is reported that the photovoltaic generator (*PVG*) is not studied in this paper, it has been replaced by a continuous voltage (V_{ac}) which is the supply voltage of the inverter. The parameter setting (k_p and k_i) of the PI controllers are shown in [17].

To test the control, we impose an active power reference equal to five point two kilowatts ($P^* = 5.2 \text{ kW}$) and the reactive power reference is equal to zero ($Q^* = 0 \text{ VAR}$). The consumption of our neighbors is modeled here by a three-phase load *RL* which consumes active power.

Thus, the following profile is considered:

- at $t \in [0 \ 0.5] \text{ s}$, the *RL* load does not consume any power of our system,
- at $t \in [0.5 \ 1] \text{ s}$, the *RL* load consumes a part of power of our system.

The simulation results of the control are shown in figures 14, 15, 16, 17 and 18.

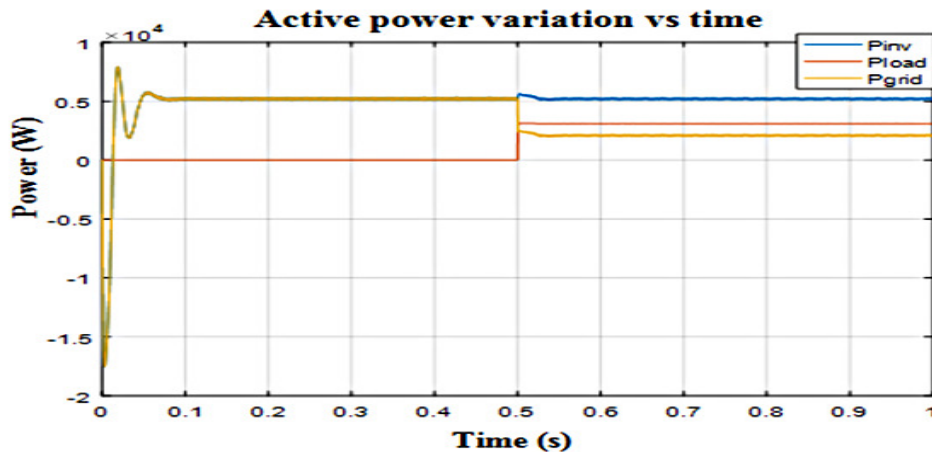


Figure 14. Active power variation

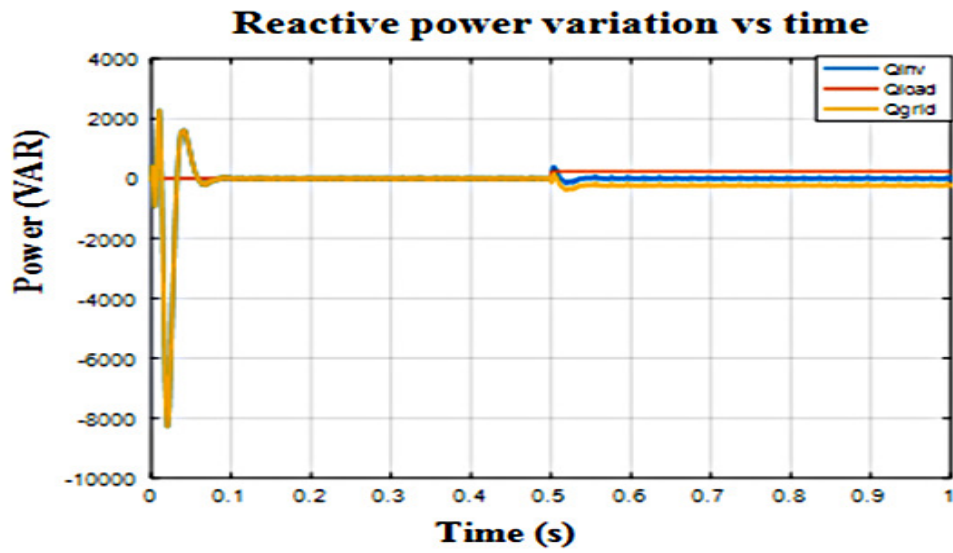


Figure 15. Reactive power variation

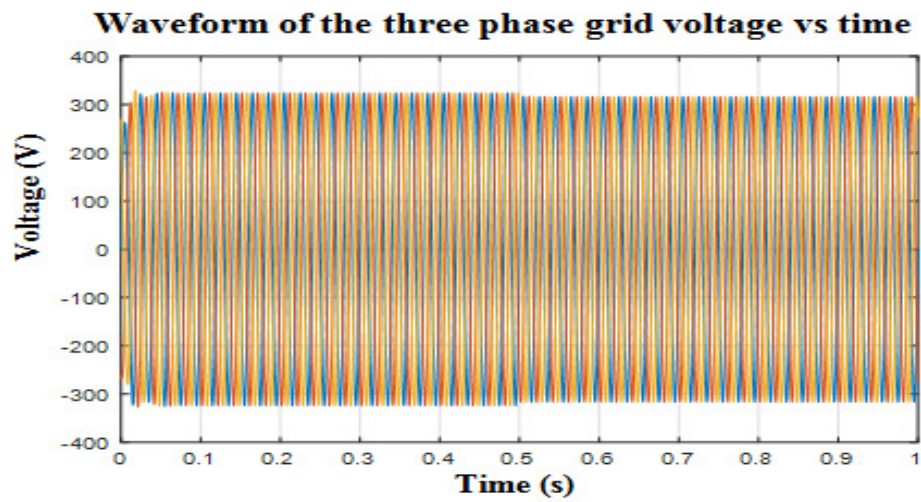


Figure 16. Wave form of the grid voltage

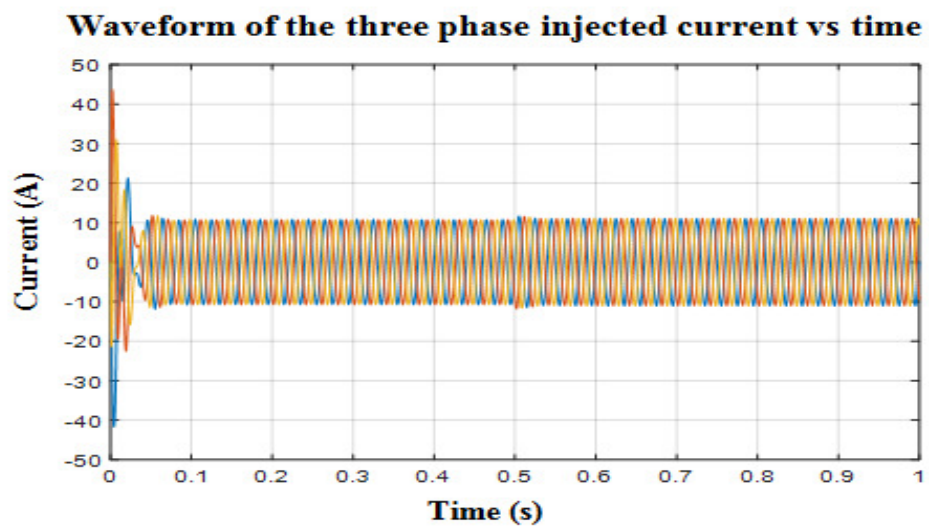


Figure 17. Wave form of the injected grid current

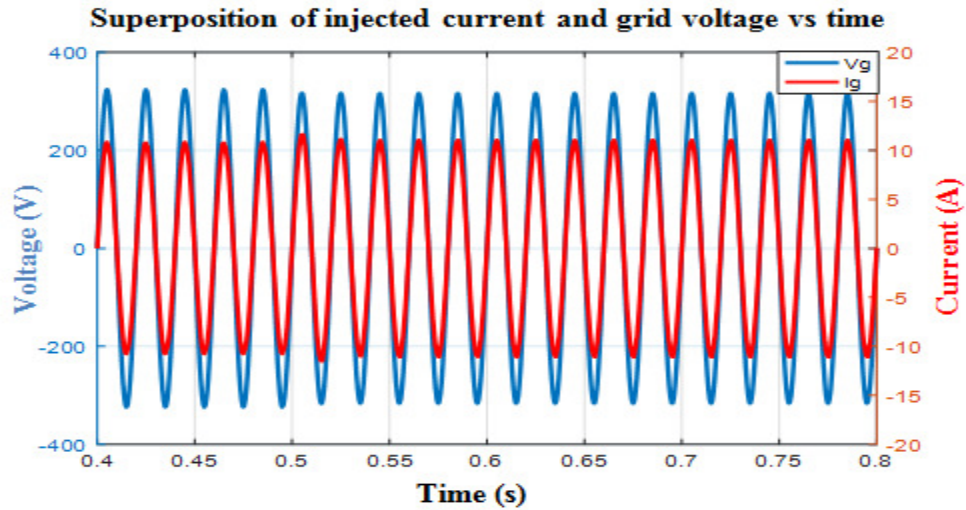


Figure 18. Synchronization of the system by PLL

6.2. Discussion

Figure 14 shows that when the active power of the load is equal to zero ($P_{load} = 0$ W) in the time interval $[0 \ 0.5]$ s, the grid active power and the inverter active power are identical ($P_{grid} = P_{inv} \approx 5.2$ kW). This means that all the power produced by our system is injected into the grid. But when the power of the *RL* load is not null ($P_{load} = 3$ kW) in the time interval $[0.5 \ 1]$ s, some of our power supplies the *RL* load and the rest of the power (2.2 kW) is injected into the grid. In figure 15, it can be seen that when the reactive power is equal to zero ($Q_{load} = 0$ VAR) in the time interval $[0 \ 0.5]$ s, our system does not inject any reactive power on the grid ($Q_{grid} = Q_{inv} = 0$ VAR). But when the load consumes power, in the interval $[0.5 \ 1]$ s, it also generates reactive power that will be injected into the grid. This is why the reactive power of the grid is slightly negative ($Q_{grid} < 0$) in this interval. Figures 16 and 17 show the grid voltage and current waveforms respectively. It can be noted that the voltage and current fluctuations due to the *RL* load are not too pronounced. Indeed, when the neighbors start to consume from our system (in the time interval $[0.5 \ 1]$ s), this results in a slight drop in voltage and a slight increase in the current in our system. However, the behavior of the transients at time $t = 0.5$ s is very interesting (so the *LCL* filter is well designed).

Figure 18 shows the superposition of the injected current on the grid ($I_g = I_2$) and the grid voltage (for one phase). It can be seen that the two curves are in phase and have the same frequency (50 Hz). Therefore, we say that our system is synchronized on the grid despite the interaction of the consumption of the neighbors on our system (at $t = 0.5$ s).

7. Conclusion and perspectives

This paper dealt with an optimized design method of an *LCL* filter for grid connected *PV* system and an analysis of the impact of the neighbor's consumption on this system. Our design complies with the *IEEE1547* standard for interconnection to the grid in terms of voltage drop, current ripples, variation in power factor (variation in reactive power) and frequency variation. The used technique to fragment the inductances with two inductances in series seems to show a gain in volume and manufacturing cost of the filter. The used

control has fulfilled its function of tracking of the references and system synchronization, when the RL load varies.

However, even if our system doesn't generate reactive power to the grid, the used control currently cannot compensate the reactive power generated obviously by the neighbours. In the future, it would be interesting to imagine a smart system that could detect reactive power at the connection point and compensate it in order to participate in a system service.

References

- [1] A. Reznik, M. S.-D. (2012). LCL Filter Design and Performance Analysis for Grid Interconnected Systems . Power Electronics and Machines in Wind Application (PEMWA), IEEE , 1-7.
- [2] BAYOUMI, E. H. (2015). Three-phase LCL-filter for Grid-connected Inverter Using Cooperative Bacteria Foraging Optimization . WESAS TRANSACTIONS ON SYSTEMES and Control , Volume 10.
- [3] M. Liserre, F. B. (2005). Design and Control of an LCL-Filter-Based Three-Phase Active Rectifier. IEEE Transactions on Industry Applications, vol. 41, no. 5, pp. 1281–1291, Sep. 2005.
- [4] Xu Renzhong, X. L. (2013). Design and Research on the LCL Filter in Three-Phase PV Grid-Connected Inverters. International Journal of Computer and Electrical Engineering, Vol. 5, No. 3.
- [5] S. V. Araujo, A. E. (2007). LCL Filter design for grid-connected NPC inverters in offshore wind turbines. The 7th International Conference on Power Electronics, October 22-26, 2007/EXCO, Daegu, Korea.
- [6] Jiri Lettl, J. B. (2011). Comparison of Different Filter Types for Grid connected Inverter. Marrakesh, MOROCCO, March 20-23: PIERS Proceedings.
- [7] Tsai-Fu Wu, S. M.-C.-W. An Improved Resonant Frequency Based Systematic LCL Filter Design Method for Grid-Connected Inverter . DOI 10.1109/TIE.2017.2682004, IEEE Transactions on Industrial Electronics.
- [8] Weimin Wu, Y. L.-H. Damping Method for Resonances Caused by LCL-filter_based current-controlled Grid-tied Power Inverters: DOI 10.1109/TIE.2017.2714143, IEEE Transactions on Industrial Electronics.
- [9] F. Hamoudi, A. M. Sliding Mod Control With Stabilized Switching Frequency for Four-Wire Shunt Active Filter. J. Electrical Systems 6-4 (2010):487-500.
- [10] Xiaoqiang Li, M.I. Active Magnetic Decoupling for Improving the Performance of Integrated LCL-Filters in Grid-Connected Converters. DOI 10.1109/TIE.2017.2733445, IEEE Transactions on Industrial Electronics.
- [11] Yong Liu, S. M.-S. LCL Filter Design of 50 kW 60 kHz SiC Inverter with Size and Thermal Considerations for Aerospace Applications. DOI 10.1109/TIE.2017.2677338, IEEE Transactions on Industrial Electronics.
- [12] H. Bekka, S. T. (2013). Power Control Of A Wind Generator Connected To The Grid In Front Of Strong Winds: J. Electrical Systems 9-3 (2013): 267-278.
- [13] IEEE Standard 1547 (2003).for Interconnecting Distributed Resources with Electric Power Systems.
- [14] M. Sarra, J.-P. G. (2014). Advanced Control Strategy of a Transformer less Three Phase Shunt Hybrid Power Filter: J. Electrical Systems 10-4 (2014): 445-455.
- [15] Forest, J.-P. F. (1999). Alimentations à découpage Convertisseurs à résonance, Principes-composants-modélisation. Livre, bibliothèque de l'ENS-CACHAN, Cachan : 3e édition DUNOD, Paris.
- [16] EPCOS. (2013). EPCOS Data Book : ferrites and accessories
- [17] Mahamat, C., Petit, M., Marouani, R., Gautier, C., Mami, A., & Costa, F. (s.d.). Decoupled PQ control applied to a multicellular parallel inverter for grid-connected photovoltaic system: IEEE Conference Publications: DOI: 10.1109/STA.2016.7952002 2016 17th International Conference on STA.
- [18] H. FERAL, T. K. (Janvier 2002). Raccordement d'une éolienne au réseau électrique d'un bâtiment. Toulouse: Rapport de Projet Long, INP- ENSEEIHT.
- [19] Nguyen, V. L. (2015). Couplage des systèmes photovoltaïques et des véhicules électriques au réseau Problèmes et solutions. Université de Grenoble: Thèse de Doctorat de l'Université de Grenoble.
- [20] LEQUEU, T. (2006). Calcul des inductances et des transformations. Cours d'Electronique de Puissance
- [21] Shahraki, E. G. (2003). Apport de l'UPFC à l'amélioration de la stabilité transitoire des réseaux électriques. Nancy: Université Henri Poincaré, Nancy-I.
- [22] Ikram Maaoui-Ben Hassine, M. W. (2015). Model Based Predictive Control For Three-Phase Grid Connected Converter. J. Electrical Systems 11-4 (2015): 463-475.
- [23] S.Z.Mohammad Noor, A. O. (2016). Single Stage String Inverter for Grid connected Photovoltaic System with Fuzzy Logic Control (FLC)-based MPPT Technique. J. Electrical Systems 12-2 (2016): 344-356.
- [24] Boualem BOUKEZATA, J.-P. G. Générateur photovoltaïque avec une commande directe de puissance connecté et avec adjonction de services au réseau de distribution. GRENOBLE: SYMPOSIUM DE GENIE ELECTRIQUE (SGE 2016) : EF-EPF-MGE 2016, 7-9 , FRANCE
- [25] Boualem Boukezata, A. C.-P. (2014). Système solaire photovoltaïque connecté au réseau électrique et associé à un filtre actif parallèle. Cachan: Symposium de Génie Electrique, Jul 2014, Cachan, France.
- [26] Rizzo, R. An integrated power converter architecture for microgrids with renewable energy sources. J. Electrical Systems 8-3 (2012): 356-366.